Original Research

Automatic Segmentation of White Matter Hyperintensities by an Extended FitzHugh & Nagumo Reaction Diffusion Model

Shuangxi Ji, MS,[1] Changqing Ye, PhD,[2] Fan Li, MD,[2] Wei Sun, MD,[2] Jue Zhang, PhD,[1,3]* Yining Huang, MD,[2]* and Jing Fang, PhD[1,3]

Purpose: To evaluate the efficiency and reproducibility of the extended FitzHugh & Nagumo (FHN) reaction-diffusion model proposed in this study for white matter hyperintensities (WMH) segmentation.

Materials and Methods: Five types of magnetic resonance T2-weighted fluid-attenuated inversion-recovery (T2FLAIR) images of 127 patients with different scanning parameters from five clinical scanner systems were selected for this study. After skull and scalp removal and denoise, the T2FLAIR images were processed by the proposed extended FHN model to obtain WMH. This new technique replaced the global threshold constant with a local threshold matrix.

Results: There was no significant difference between the segmentation results of the training set and the manual contouring against those between the test set and the manual contouring based on similarity index (SI) values ($P = 0.5217$). The SI values of the five types of T2FLAIR images were 86.0% ± 15.4%, 85.8% ± 10.5%, 84.1% ± 14.8%, 87.2% ± 14.6%, 86.3% ± 12.7%, respectively, comparing the segmentation results using the proposed method to the manual delineations. The overall SI value of the images was 86.5% ± 14.5%. This approach also demonstrated a better WMH segmentation performance over its classic form ($P < 0.001$).

Conclusion: The proposed approach is efficient and could provide a more effective and convenient tool for clinical quantitative WMH analysis.

Key Words: white matter hyperintensities; FitzHugh & Nagumo model; automatic segmentation; similarity index
J. Magn. Reson. Imaging 2013;37:343–350.

WHITE MATTER HYPERINTENSITIES (WMH) are attracting increasing attention from researchers worldwide. They are commonly found on magnetic resonance (MR) images of the elderly with diseases including cerebral vascular disorders (eg, stroke (1,2), Alzheimer's syndrome (3–6)), autoimmune diseases (eg, multiple sclerosis (7,8)), neurodegenerative diseases (eg, dementia (1,9,10)), etc. Besides correlation with advanced age, they might be seen in patients with gait and balance dysfunction (11) and carbon monoxide poisoning (12). Although WMH is also often present in healthy elderly individuals, studies have shown that they are related to deficits in speed of cognitive processing (13). MR T2 weighted fluid-attenuated inversion recovery (T2FLAIR) imaging offers advantages over other imagings for detecting WMH because of the high contrast between WMH and other brain tissues.

It has been realized that the number, size, and location of WMH in MR images could provide valuable information to explore the etiology and the development of disease, and to evaluate the therapeutic effect of treatment. In fact, both qualitative and quantitative analysis techniques have been used to measure WMH load in clinical practice. For qualitative analyses, visual rating scales, which are operationally defined in MRI (14–16), have been frequently used by well-experienced doctors to grade the severity of WMH. Although quick and convenient, that method sometimes could not achieve high consistencies among longitudinal studies due to the subjectivity of observers (16). Moreover, the visual rating scale approach oftentimes does not provide enough accuracy because of its relatively large measurement units (ie, categories) and poor sensitivity to lesion size.

The quantitative analysis approaches for WMH segmentations vary from fully manual contouring techniques to fully automatic segmentation. In fully manual

[1]College of Engineering, Peking University, Beijing, China.
[2]Department of Neurology, Peking University First Hospital, Beijing, China.
[3]Academy of Advanced Interdisciplinary Study, Peking University, Beijing, China.
Contract grant sponsor: Fundamental Research Funds for the Central Universities and the 5th Five-year Project grant from the Ministry of Science and Technology of the People's Republic of China; Contract grant number: 2008ZX09312-017.
*Address reprint requests to: J.Z., College of Engineering, Peking University, No.5 Yiheyuan Road Haidian District, Beijing, China 100871. E-mail: zhangjue@pku.edu.cn or Y.H., Dept. of Neurology, Peking University First Hospital, No.8 Xishiku Street, Xicheng District, Beijing, China, 100034. E-mail: ynhuang@sina.com
Received February 2, 2012; Accepted August 24, 2012.
DOI 10.1002/jmri.23836
View this article online at wileyonlinelibrary.com.

strategies (17,18) the WMH boundaries of the image displayed on-screen are first manually traced by the doctor. Then the pixel number of the region of interest (ROI) is calculated by computer. Finally, the volume of lesion is yielded by considering the thickness of each slice. These procedures are easy to follow and provide accurate and consistent results. However, they are time-consuming and require operators with rich experience in segmentation.

Many semiautomatic strategies have been proposed by some researchers (19–23). For instance, in the approach developed by Hirono et al (23), they manually traced the rough contours of ROIs and then to define WMH whose gray level value was above a certain threshold in the selected region. The threshold was chosen to be the standard deviation of the normal white matter obtained in the MR T1 images. Although more efficient than manual contouring, these semiautomatic methods were not always feasible when a large number of images were involved. In that case, user intervention during segmentation was still necessary. Among the fully automatic techniques, Lao et al (24) proposed an approach based on Support Vector Machine for the segmentation of WMH in MR images. Admiraal-Behloul et al (25) and Gibson et al (26) introduced the Fuzzy C-Means cluster method to automatically segment WMH. Van Leemput et al (27) presented an algorithm based on a Gaussian model, which described intensity-based brain tissues and detected lesions by searching for the outliers of the model.

Generally, for image segmentations the available approaches mentioned above were all developed on the basis of the intensity information of original images. The local spatial information, which represents the relationship between neighboring pixels, has not been effectively taken into account in many cases. As we know, WMH always present irregular shapes, and the boundaries between WMH and surrounding normal tissues usually have a rather fuzzy distribution. As a consequence, those conventional WMH segmentation techniques are prone to the effect of noise, and inevitably yield inconsistent results in different measurements.

For years, researchers have attempted to apply the reaction diffusion (RD) models to image processing via image evolution and have achieved many favorable results. RD models were originally developed to simulate the natural process in which both the reaction between the substances and the diffusion of the substances coexist. The models have been found to be closely related with the natural pattern formation process. This fact enabled their applications in image processing due to their capability of utilizing both intensity and spatial information (28–33) in the pattern distribution. Indeed, compared to conventional methods, the RD model-based approaches are able to detect the boundaries of images with higher efficiency in the presence of small intensity gradients (30), which makes it more adaptive to deal with the images with fuzzy outlines. One of the most widely adopted RD models is the FitzHugh & Nagumo model (FHN), characterized by its reaction term to simulate both the activation and inhibition dynamics of the system. It was first introduced to simulate the propagation of active electrical pulses along a nerve axon in 1962 (34,35). In recent progress of image processing, Ebihara et al (31) studied the FHN model and presented the conditions for stable results in edge detection and image segmentation; Liu et al (32) proved its validity in noise reduction; and Miura et al (33) employed it to extract features in 3D images, etc.

The purpose of this study was to apply the FHN based segmentation method for fully automatic WMH detection on MR T2FLAIR images. In this work, we extended the classical FHN-based segmentation method by replacing the threshold constant a with a matrix A, which represents a local threshold adaptively determined from the gray levels of the neighboring pixels within the area with WHM and normal brain tissues. To evaluate the proposed adaptive segmentation technique, five types of T2FLAIR images with different scanning parameters of 127 patients with WMH were investigated and the final automatically explored lesions were compared to manually measured WMH by three experienced doctors.

MATERIALS AND METHODS

Patients and Scanning Protocol

This study was approved by the Institutional Review Board. Written informed consent was obtained. MR T2FLAIR images of 127 patients diagnosed with white matter disease who were examined from 2004 to 2006 were included in the study. None of these patients showed manifestations of serious or moderate disability in accordance with the Instrumental Activities of Daily Living scale (36). The datasets were acquired with five clinical MR scanners: General Electric (GE, Milwaukee, WI) Signa 1.5 T, GE Signa 3.0 T, Siemens (Erlangen, Germany) Sonata 1.5 T, Philips (Eindhoven, Netherlands) Gyroscan Intera 1.0 T, and Philips Gyroscan Intera 1.5 T. For each participant the dataset was compiled with a single scanner. According to the scanning parameters, the T2FLAIR images can be divided into five types (Table 1).

Data Quality Assessment

Before processing T2FALIR images, all MRI datasets were evaluated in order to achieve a more homogenous quality level. The images were excluded from further participation if 1) there were no WMH in the image, 2) artifacts were present. After data quality assessment, there were 997 T2FLAIR images from 127 patients left (Table 2).

Segmentation Method

Image Preprocessing

Before using the FHN model to segment WMH, skull and scalp regions were removed from T2FLAIR images using the brain extraction tool (BET, Smith 2002). Then an anisotropic diffusion equation (37) (15 iterations, time step = 0.2, conduction coefficient $K = 30$;

Table 1
Characteristics of the Five Types of T2FLAIR Images

T2FLAIR[a] Images type	MR scanner type	Number of patients[c]	Age of patients (y)[d]	Matrix size	Repetition time (msec)	Echo time (msec)	Number of slices	Slice thickness (mm)	Field of view (mm)
I	GE[b] Signa 1.5 T	36 (28M/8F)	63.5 ± 9.8	256 × 256	9002	2200	18	6	240 × 240
II	GE Signa 3.0 T	22 (18M/4F)	61.2 ± 9.4	512 × 512	9002	2250	18	6	240 × 240
III	Siemens Sonata 1.5 T	17 (10M/7F)	59.4 ± 10.8	416 × 512	10000	2500	18	6.5	240 × 240
IV	Philips Gyroscan Intera 1.0T	36 (22M/14F)	63.3 ± 9.0	512 × 512	6000	1900	14	6	240 × 240
V	Philips Gyroscan Intera 1.5T	16 (11M/5F)	63.6 ± 14.9	256 × 256	7000	2000	14	6	240 × 240
Overall	NA	127 (89M/38F)	62.1 ± 10.4	NA	NA	NA	NA	NA	NA

[a]T2FLAIR, T2 weighed fluid-attenuation inversion-recovery.
[b]GE, General Electric.
[c]F, female, M, male.
[d]Data are shown as mean plus-minus standard deviation.NA, not applicable.

these values were determined based on trial and error) was employed to denoise and smooth the signal.

Classic and Extended FHN Model

The classic FHN RD model consists of two partial differential equations:

$$\begin{cases} \frac{\partial u}{\partial t} = D_u \Delta u + \frac{1}{\varepsilon}(u(u-a)(1-u) - v) \\ \frac{\partial v}{\partial t} = D_v \Delta v + (u - bv) \end{cases} \quad [1]$$

where $\epsilon(0 < \epsilon \ll 1)$ is a small positive constant, describing the time scale relationship between the variables u and v. $a(0 < a < 1)$, $b(b > 0)$ are constants. $D_u\Delta u$ and $D_v\Delta v$ are the diffusion terms in which D_u and D_v are the diffusion coefficients. $\frac{1}{\varepsilon}(u(u-a)(1-u)-v)$ and $(u - bv)$ are the reaction terms (for detailed explanation, please refer to (30)).

It is worth mentioning that in this study the constant a in the classic FHN model was extended to a matrix named A with the same size as the image to be segmented. That is, for a given T2FLAIR image whose size is $M \times N$, A is also an $M \times N$ matrix. The construction of A is as follows. We first scale the preprocessed T2FLAIR image matrix to (0, 1) to get its normalized form I_0. $H(i,j)$ is the average of $I_0(i,j)$ and its eight neighborhoods. Here $1,\ldots,M$; $j = 1,\ldots,N$. We set $A(i,j) = k \times H(i,j)$. If $A(i,j) = s \times \mathrm{STD}(I_0)$, then we reset the value of the element as $= s \times \mathrm{STD}(I_0)$. $\mathrm{STD}(I_0)$ is the standard deviation of I_0. k and s are constants with empirical values.

Segmentation Process

Since the model has some adjustable parameters (D_u,D_v,b,ϵ,k,s), we used about one-third of the data (330 T2FLAIR images) as a training set to obtain optimized values. These images were chosen arbitrarily. The other data were employed as a test set. The segmentation scheme of the proposed approach included four steps, as demonstrated in Fig. 1.

Step 1: Using the preprocessed T2FLAIR image to obtain the matrix A with certain values of k and s.

Step 2: Substituting matrix A into Eq. [1] and selecting parameters D_u, D_v, b, ϵ with some values. The initial conditions and boundary conditions for the two variables (u, v) are no-flux Neumann boundary conditions given by Eqs. [2] and [3], respectively:

$$\begin{cases} u_0 = I_0 \\ v_0 = 0 \end{cases} \quad [2]$$

$$\begin{cases} \partial u/\partial n = 0 \\ \partial v/\partial n = 0 \end{cases} \quad [3]$$

where n is the normal to the boundary of the image to be processed.

Step 3: Using the finite difference scheme to find the numerical solution of u and v with the discrete space step h and time step τ, respectively. Fixed values utilized for these two parameters were $h = 1$, $\tau = 0.01$.

Step 4: Via image evolution flows, finally transforming the converged matrix u into the segmentation result. The convergence can be confirmed by verifying that the mean square error between the results of two nearby iterations is less than a given small value ϵ. (In this study, ϵ was chosen empirically as 0.001.).

Step 5: Reselecting values of these parameters in their respective ranges and comparing the automatic segmentation results with manual delineation using similarity index (SI) described in the Evaluation section. The highest SI corresponds to the optimized values of the parameters.

Table 2
Data Quality Assessment of the Five Types of T2FLAIR Images

T2FLAIR images type	T2FLAIR images	images without WMH	images of artifacts presented[a]	T2FLAIR images remained[b]
I	648	314	48	286
II	396	137	31	228
III	306	115	26	165
IV	504	232	39	133
V	224	114	25	185
Overall	2078	872	209	997

[a]They were counted within the T2FLAIR images with WMH.
[b]There was no patient whose images were all ruled out.

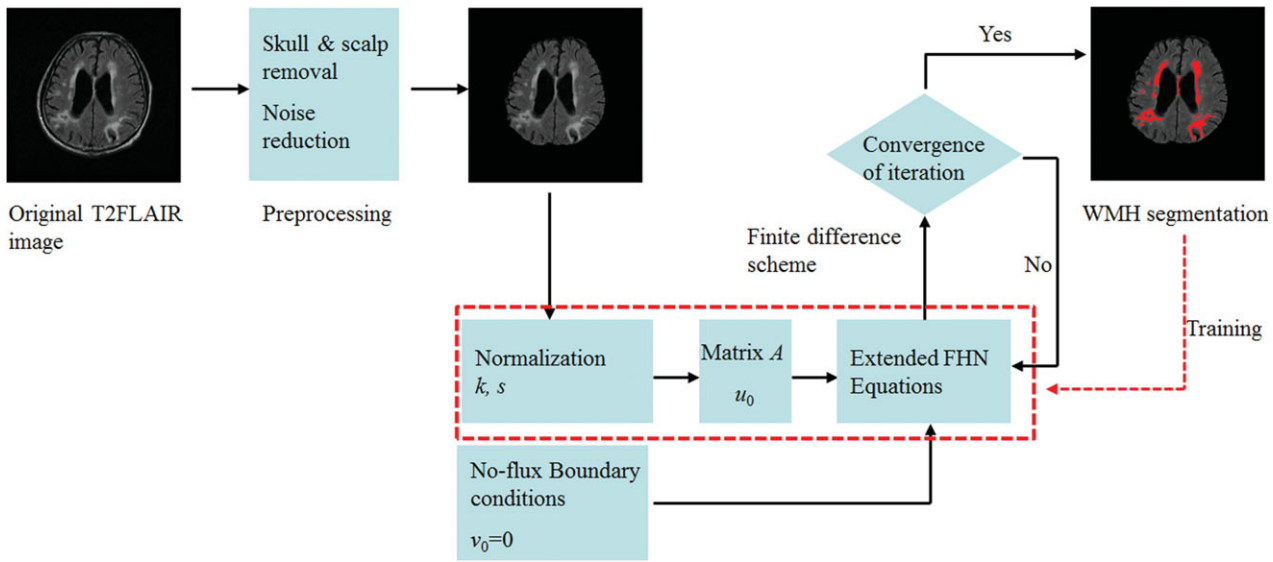

Figure 1. The total segmentation scheme based on the extended FHN model.

After training, we got: $D_u = 0.1$, $D_v = 10$, $b = 20$, $\epsilon = 0.0001$, $k = 0.95$, $s = 6.5$. The whole image preprocessing and WMH segmentation processes were done with the help of MatLab (MathWorks, Natick, MA) software.

Evaluation

To evaluate the results processed using the proposed method, the SI expressed in the following equation is calculated to measure the coincidence degree of the segmentation results between the presented technique and the manual approach (38), given by:

$$\mathrm{SI} = \frac{2|\mathrm{A} \cap \mathrm{M}|}{\mathrm{A} + \mathrm{M}} \times 100\% \qquad [4]$$

where M is the manual delineation result of each slice. It was generated by a consensus of three clinical neurology experts and each had more than 10 years' experience in WMH diagnosis. They used PhotoShop (Adobe, San Jose, CA) to generate WMH masks. The lasso tool was used to trace the edges and the eraser tool was applied to set the parts in the contours to foreground and others background. A stands for the automatic segmented result of each slice using the proposed method; A∩M represents the number of identical pixels between A and M. SI takes values between 0 and 100%, in which zero means no overlap at all (total disagreement) and 100% means an ideal agreement between the two results. An SI value of 70% or higher indicates very good to excellent agreement (39).

Finally, to estimate the improvement in the FHN model from a fixed threshold to an adaptive threshold matrix that was proposed in this study, we iterated the preset threshold a from 0 to 1 with a step of 0.05, and the independent samples t-test of SI value with 95% confidence interval was used to verify the significance of the segmentation difference between the two strategy groups.

RESULTS

Figure 2 shows the evolution of the WMH segmentation process by employing the extended FHN model. The variable u related to the image intensity distribution converges quickly to WMH regions after a few iterations within several seconds of computation time in the modified model. The segmentation examples using both the automatic method and manual delineation are demonstrated in Fig. 3. Four original T2FAIR images chosen randomly from the test set are given in Fig. 3a. The corresponding WMH segmentation results by using the proposed method and manual delineation overlapping with the preprocessed T2FLAIR images are displayed in Fig. 3b,c, respectively. The SI values between the automatic segmentation results and the manually generated results are

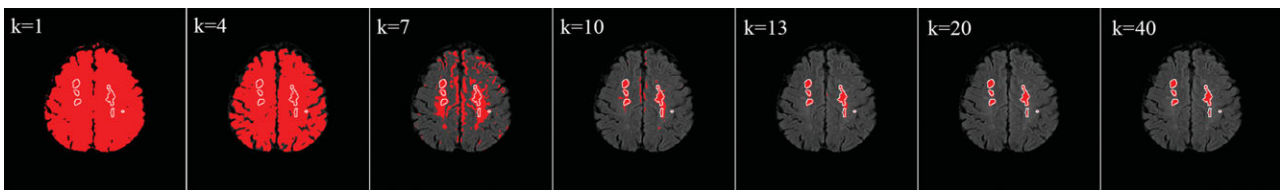

Figure 2. The evolution result of the variable u with different iteration number k. From left to right, k is taken as 1, 4, 7, 10, 13, 20, 40.

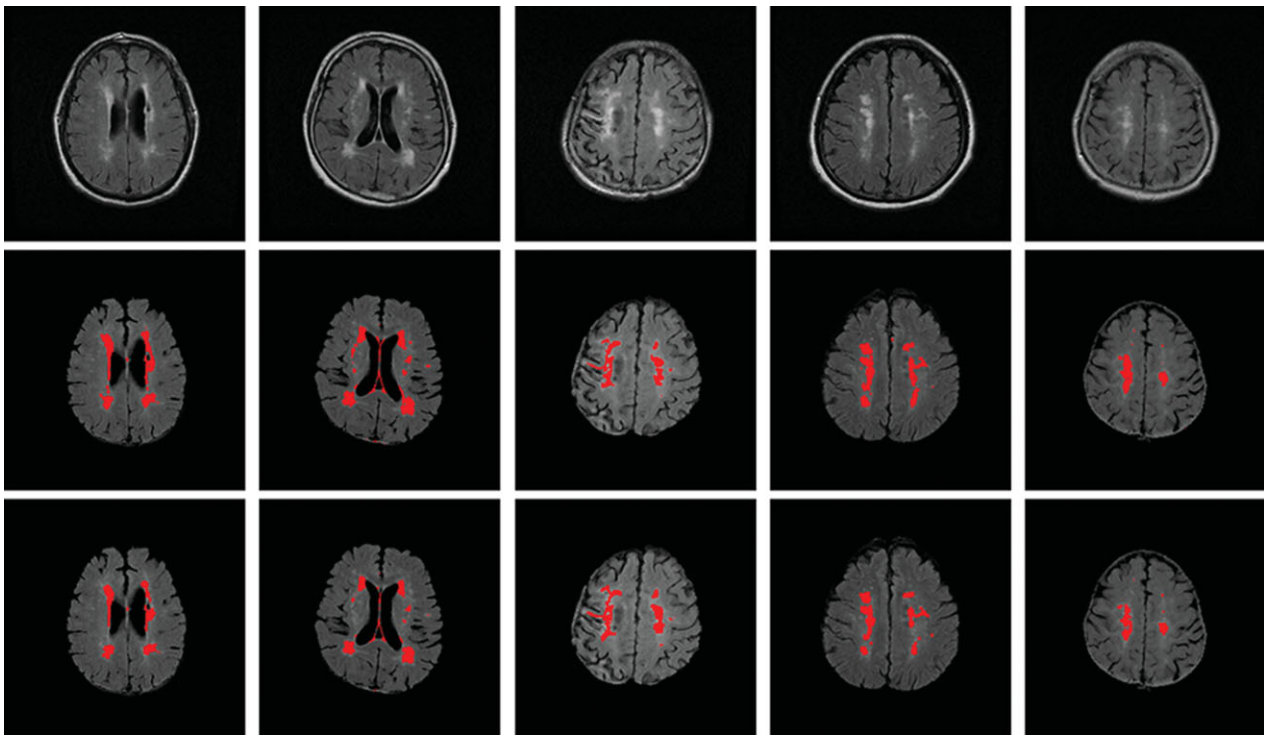

Figure 3. The comparison of the automatic segmentation results and manual delineation. **a**: Original T2FAIR images. **b**: Segmented results obtained by using the extended FHN model overlapping with the preprocessed T2FLAIR images. **c**: Manual contouring results overlapping with the preprocessed T2FLAIR images. [Color figure can be viewed in the online issue, which is available at wileyonlinelibrary.com.]

show in Table 3. There is no significant difference between the segmentation results of the training set and the manual contouring against those between the test set and the manual contouring based on SI values ($P = 0.5217$). Moreover, we also calculated the SI values between the segmentation results using the classic FHN model and the manually delineated results, as plotted in Fig. 4a. In the classic model, the threshold a varies from 0 to 1 with a step of 0.05. It is observed that compared to the classic method, the extended FHN model with the adaptive threshold matrix A presents a significantly higher SI value in WMH segmentation results (Fig. 4b) (maximal $P < 0.001$ at $a = 0.75$).

DISCUSSION

In this study an automatic WMH segmentation method is proposed using an extended FHN model. The automatically segmented results were validated against manually drawn WMH on five types of T2FLAIR images from the 127 patients. Although each type of image is from a different MR scanner and have different scanning parameters, the SI values of the segmentation results between the proposed approach and the standard manual contouring method indicate a good agreement in the sizes and locations of the WMH. This new method also yields relatively low false positives: I, 9.5% ± 16.5%; II, 9.1% ± 14.5%; III, 14.7% ± 17.6.0%; IV, 11.4% ± 18.6%; V, 9.5 ± 16.1%. The false positive was calculated referring to the literature (26).

In fact, The FHN model was originally derived from the two-component reaction diffusion equations. It simulates a system with both the activation and deactivation mechanisms. The two variables u and v symbolize the "activator" and "inhibitor" forces in the system. An important characteristic of the original FHN model is that under a certain condition, that is, when the "activator" u exceeds a certain threshold a, the system will evolve into a stable state by exhibiting a characteristic excursion in its phase space. As analyzed in the literature (30–33), the thresholding process enables its applications in image segmentation, as it is able to cluster the pixels into two groups: the foreground and background after finite iterations, the parameter a in the classic FHN model corresponds to the segmentation threshold. In addition, this method takes into account the spatial information of the

Table 3
Values of Similarity Index Comparing the Automatic Segmentation Results Using the Extended FNH Model to the Manually Generated Results

T2FLAIR[a] Images type	SI[b] value
I	86.0% ± 15.4%
II	85.8% ± 10.5%
III	84.1% ± 14.8%
IV	87.2% ± 14.6%
V	86.3% ± 12.7%
Overall	86.5% ± 14.5%

[a]T2FLAIR= T2 weighed fluid-attenuation inversion-recovery.
[b]SI, similarity index, data are shown as mean plus-minus standard deviation.

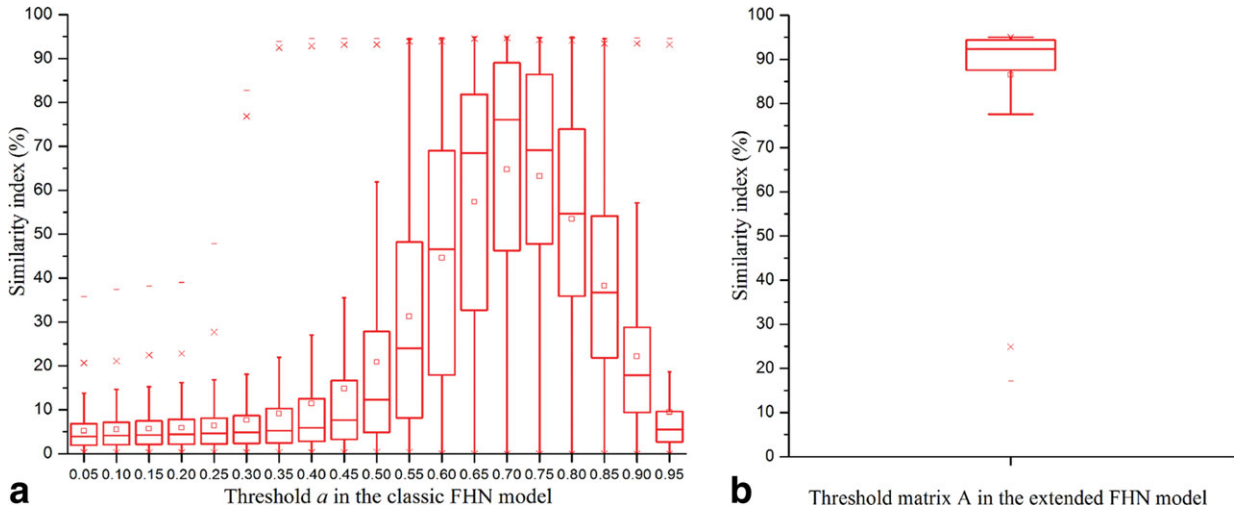

Figure 4. Comparison of WMH segmentation results achieved by the classic FHN model and the proposed extended FNH model. **a**: The SI values based on the classic FHN model in which the threshold a varies from 0 to 1.0 with a step of 0.05. **b**: The SI value by using the extended FNH model with an adaptive threshold matrix A. [Color figure can be viewed in the online issue, which is available at wileyonlinelibrary.com.]

pattern distribution, which makes it more suitable to outline objects with fuzzy edges.

In most available applications of FHN models in image segmentation, a single constant threshold a is usually applied. The premise of a successful segmentation of the WMH using the FHN model is that the local threshold is within the range determined by the gray level values of WMH and normal brain tissues. However, in the case of T2FLAIR images of WMH, due to the gray level intensity inhomogeneity among different T2FLAIR images and within a given T2FLAIR image, this premise cannot always be satisfied. As a consequence, a single global threshold a does not provide satisfactory segmentation results. In this study, the single constant a in the classic FHN model was extended to a matrix named A to adaptively detect WMH. Based on local intensity distribution of the normalized preprocessed T2FLAIR image, the adaptive threshold of each pixel is represented by a corresponding element in the matrix A. Specifically, in this work, each element of matrix A was first constructed using the local average of the normalized intensity (within a 3-by-3 neighborhood) multiplying a coefficient k which is less than one. If we only do so, most of pixels will turn out to be foreground due to their intensities being higher than each corresponding threshold. We found that the averaged intensities of normal brain tissues are approximately proportional to STD(I_0). So a proper value of parameter s can be chosen in order to make $s \times$ STD(I_0) be between the intensity of normal brain tissues and WMH. In addition, when we fixed this value of s, the situation also could be obtained for most other images. Now, $A(i,j)$ is reassigned to $s \times$ STD(I_0) if any $A(i,j) < s \times$ STD(I_0). Here we should note that the intensities of almost all of the background and normal tissue are lower than their new threshold and, on the contrary, most of the WMH pixels have the converse situation. Thanks to the efficiency of clustering fuzzy objects of the FHN model in image processing (30), the former will evolve to the new background after a limited number of iterations in Step 4 and the latter will be left out as the foreground.

It is worth mentioning that we did not correct the bias field which leads to a smoothly varying intensity inhomogeneity for the same tissue over an entire MR image. Bias field correction may help achieve better performance of our method. However, this operation would increase computational complexity and time cost. Moreover, since our proposed model has an adaptive threshold matrix, it isn't quite sensitive to the intensity in-homogeneities.

It also has to be mentioned that the thresholding process involved in the proposed method is essentially different from the traditional thresholding technique, which is widely applied in classical segmentation algorithms. And it differs from the fuzzy connectedness technique put forward by Udupa et al (21) for multiple sclerosis delineation as well, which also employs spatial information for image segmentation. In the conventional thresholding method a successful edge-detection operation requires a significant contrast between the foreground and background in a histogram. However, this condition cannot always be satisfied for most clinical T2FLAIR images, which oftentimes have fuzzy and blurry edges. In addition, for many clinical images with multiple intensity levels, local contrast cannot indeed be reflected in a histogram. As a consequence, these methods inevitably lead to under- or overestimated results. The idea of the fuzzy connectedness is based on the principle that the object information in images is fuzzy and has a special connectedness, which is also fuzzy. In practice, one computes a map of the connectedness of every pixel in the original image in relation to a specific pixel (manually designated) belonging to the object of interest. The neighboring connectedness or affinity between two pixels is defined via a function that indicates the degree of adjacency and the similarity of their intensity values. Once the map is computed, the

segmented object is obtained by the simple thresholding method. Although the practical results of segmentation obtained by this method are good in some cases, it also has some weaknesses: It is a semiautomatic technique where the operator needs to allocate special points on the objects of interest and the segmentation results strongly depend on the affinity function defined and the choice of the threshold used for the binarization of the connectedness map. In our work, through combining the adaptive threshold matrix and the FHN model, the mutual interaction between the reaction term and diffusion term at a local area in a given image, the extended FHN utilizes the spatial and intensity distribution information in its nonlinear dynamical evolution. Namely, with the blurry interfaces between WMH and normal brain tissue being gradually highlighted, the lesion border at the stable or converged state from T2FLAIR images is finally extracted.

This study is certainly not without limitations. Although T2FLAIR provides the best contrast between normal tissue and WMH compared to other imaging technologies, it may overestimate lesion load, which usually appears on the edge of the lateral ventricle region. Previous researchers have reported that proton density weighted images may be effective in eliminating these false positives (24). Therefore, multicontrast images could be taken into consideration to improve the lesion segmentation performance in future work.

In summary, we have demonstrated an extended FHN model with a threshold matrix to automatically segment WMH on five types of T2FLAIR images. The WMH segmentations are consistent with those from manual delineations based on SI evaluations. These results suggest that the proposed approach provides a more effective and convenient tool for clinical quantitative WMH analysis.

REFERENCES

1. Debette S, Markus HS. The clinical importance of white matter hyperintensities on brain magnetic resonance imaging: systematic review and meta-analysis. BMJ 2010;341:c3666.
2. Vermeer SE, Hollander M, van Dijk EJ, Hofman A, Koudstaal PJ, Breteler, MM. Silent brain infarcts and white matter lesions increase stroke risk in the general population: the Rotterdam Scan Study. Stroke 2003;34:1126–1129.
3. Hirono N, Kitagaki H, Kazui H, Hashimoto M, Mori E. Impact of white matter changes on clinical manifestation of Alzheimer's disease. Stroke 2000;31:2182–2188.
4. de Leeuw FE, de Groot JC, Achten E, et al. Prevalence of cerebral white matter lesions in elderly people: a population based magnetic resonance imaging study. The Rotterdam Scan Study. J Neurol Neurosurg Psychiatry 2001;70:9–14.
5. Frisoni, GB, Galluzzi S, Pantoni L, Filippi M. The effect of white matter lesions on cognition in the elderly—small but detectable. Nat Clin Pract Neurol 2007;3:620–627.
6. Scheltens P, Barkhof F, Valk J. White matter lesions on magnetic resonance imaging in clinically diagnosed Alzheimer's disease: evidence for heterogeneity. Brain 1992;115:735–748.
7. Sajja BR, Datta S, He R, et al. Unified approach for multiple sclerosis lesion segmentation on brain MRI. Ann Biomed Eng 2006; 34:142–151.
8. Khayati R, Vafadust M, Towhidkhah F, Nabavi M. Fully automatic segmentation of multiple sclerosis lesions in brain MR T2FLAIR images using adaptive mixtures method and Markov random field model. Comput Biol Med 2008;38:379–390.
9. Schneider JA, Wilson RS, Cochran EJ, et al. Relation of cerebral infarctions to dementia and cognitive function in older persons. Neurology 2003;60:1082–1088.
10. Prins ND, van Dijk EJ, den Heijer T, et al. Cerebral white matter lesions and the risk of dementia. Arch. Neurol 2004;61: 1531–1534.
11. Guttmann, CRG, Benson R, Warfield SK, et al. White matter abnormalities in mobility-impaired older persons. Neurology 2000;54:1277–1283.
12. Parkinson RB, Hopkins RO, Cleavinger HB, et al. White matter hyperintensities and neuropsychological outcome following carbon monoxide poisoning. Neurology 2002;58: 1525–1532.
13. Nordahl CW, Ranganath C, Yonelinas AP, Decarli C, Fletcher E, Jagust WJ. White matter changes compromise prefrontal cortex function in healthy elderly individuals. J Cogn Neurosci 2006;18: 418–429.
14. Scheltens P, Erkinjunti T, Leys D, et al. White matter changes on CT and MRI: an overview of visual rating scales. European task force on age-related white matter changes. Eur Radiol 1998;39: 80–89.
15. Yue N, Arnold A, Longstreth W, et al. Ventricular and white matter changes at MR imaging in the aging brain: data from the Cardiovascular Health Study. Radiology 1998;202:33–39.
16. Mäntylä R, Erkinjuntti T, Salonen O, et al. Valuable agreement between visual rating scales for white matter hyperintensities on MRI comparison of 13 rating scales in a poststroke cohort. Stroke 1997;28:1614–1623.
17. Grimaud J, Lai M, Thorpe, J, et al. Quantification of MRI lesion load in multiple sclerosis: a comparison of three computer-assisted techniques. Magn Reson Imaging 1996;14: 495–505.
18. Bryan R, Manolio T, Schertz L, et al. A method for using MR to evaluate the effects of cardiovascular disease on the brain: the Cardiovascular Health Study. Am J Neuroradiol 1994;15: 1625–1633.
19. Filippi M, Horsfield MA, Bressi S, et al. Intra-and inter-observer agreement of brain MRI lesion volume measurements in multiple sclerosis. Brain 1995;118:1593–600.
20. Guttmann CRG, Kikinis R, Anderson MC, et al. Quantitative follow-up of patients with multiple sclerosis using MRI: reproducibility. J Magn Reson Imaging 1999;9:509–528.
21. Udupa JK, Wei L, Samarasekera S, Miki Y, van Buchem MA, Grossman RI. Multiple sclerosis lesion quantification using fuzzy-connectedness principles. IEEE Trans Med Imaging 1997;16: 598–609.
22. Makale M, Solomon J, Patronas Nj, Danek A, Butman JA, Grafman J. Quantification of brain lesions using interactive automated software. Behav Res Methods Instrum Comput 2002;34: 6–18.
23. Hirono N, Kitagaki H, Kazui H, Hashimoto M, Mori E. Impact of white matter changes on clinical manifestation of Alzheimer's disease. Stroke 2000;31:2182–2188.
24. Lao Z, Shen LD, Jawad AF, et al. Computer-assisted segmentation of white matter lesions in 3D MR images using support vector machine. Acad Radiol 2008;15:300–313.
25. Admiraal-Behloul F, van den Heuvel DMJ, Olofsen H, et al. Fully automatic segmentation of white matter hyperintensities in MR images of the elderly. NeuroImage 2005;28:607–617.
26. Gibson E, Gao F, Black SE, and Lobaugh, NJ. Automatic segmentation of white matter hyperintensities in the elderly using T2FLAIR images at 3T. J Magn Reson Imaging 2010;31: 11–1322.
27. Van Leemput K, Maes F, Vandermeulen D, et al. Automated segmentation of multiple sclerosis lesions by model outlier detection. IEEE Trans Med Imaging 2001;20:677–688.
28. Price CB, Wambacq P, Oosterlinck A. Applications of reaction-diffusion equations to image processing. In: 31st Int Conf Image Proc Appl; Warwick, UK, 1989.
29. Price CB, Wambacq P, Oosterlinck A. Image enhancement and analysis with reaction-diffusion paradigm. Proc Inst Elect Eng 1990;137:136–145
30. Nomura A, Ichikawa M, Okada K, Miike H, Sakurai T. Edge detection algorithm inspired by pattern formation processes of reaction-diffusion systems. Int J Circuits Syst Sign Process 2010; 5:105–115.

31. Ebihara M, Mahara H, Sakurai T, Nomura A, Miike H. Image processing by a discrete reaction-diffusion system. In: Proc 3rd IASTED Int Conf Visual Imaging Image Proc 2003;448–453.
32. Liu F, Ha Y. Noise reduction based on reaction-diffusion system. In: Proc 2007 Int Conf Wavelet Anal Pattern Recogn; Beijing, China 2007;2–4.
33. Miura K, Osa A, Miike H. Self-organized feature extraction in a three-dimensional discrete reaction-diffusion system. Lett Forma 2008;23:19–23.
34. FitzHugh R. Impulses and physiological states in theoretical models of nerve membrane. Biophys J 1961;45–466.
35. Nagumo J, Arimoto S, Yoshizawa S. An active pulse transmission line simulating nerve axon. Proc I R E 1962;50:2061–2070.
36. Pantoni L, Basile AM, Pracucci G, et al. Impact of age-related cerebral white matter changes on the transition to disability—the LADIS study: rationale, design and methodology. Neuroepidemiology 2005;24:51–62.
37. Perona P, Malik J. Scale-space and edge detection using anisotropic diffusion. IEEE Trans Pattern Anal Mach Intell 1990;12: 629–639.
38. Bartko JJ. Measurement and reliability: statistical thinking considerations. Schizophr Bull 1991;17:483–488.
39. Zijdenbos AP, Dawant BM, Margolin RA, Palmer AC. Morphometric analysis of white matter lesions in MR images: method and validation. IEEE Trans Med Imaging 1994;13: 716–724.